

# SystolicAttention: Fusing FlashAttention within a Single Systolic Array

Jiawei Lin

jiawei.lin@epfl.ch

EPFL

Lausanne, Switzerland

Yuanlong Li

yuanlong.li@epfl.ch

EPFL

Lausanne, Switzerland

Guokai Chen

guokai.chen@epfl.ch

EPFL

Lausanne, Switzerland

Thomas Bourgeat

thomas.bourgeat@epfl.ch

EPFL

Lausanne, Switzerland

## Abstract

Transformer models rely heavily on scaled dot-product attention (SDPA), typically implemented using the FlashAttention algorithm. However, current systolic-array-based accelerators face significant challenges when executing FlashAttention. Systolic arrays can only achieve high utilization for consecutive and large matrix multiplications. In contrast, FlashAttention requires frequently interleaved matrix multiplications and softmax operations.

The frequent data swaps between the systolic array and external vector units result in low systolic array utilization. This is further exacerbated by the fact that softmax involves numerous non-matrix operations, which are not well-suited for systolic arrays. Moreover, the concurrent execution of matrix multiplication on systolic arrays and softmax on vector units leads to register file and SRAM port contention, further degrading performance.

To overcome these limitations, we propose FSA, an enhanced systolic array architecture that enables the entire FlashAttention algorithm to run entirely within a single systolic array—eliminating the need for external vector units. At the core of FSA is SystolicAttention, a novel scheduling algorithm that maps FlashAttention operations onto systolic arrays with fine-grained, element-wise overlap. This significantly improves array utilization while preserving the original floating-point operation order to maintain numerical stability.

We implement FSA in synthesizable RTL and evaluate its performance against state-of-the-art commercial accelerators. Our results show that FSA achieves 1.77 $\times$  and 4.83 $\times$  higher attention FLOPs/s utilization compared to AWS NeuronCore-v2 and Google’s TPUv5e, respectively, with only about 10% area overhead.

## Keywords

Systolic Array, Flash Attention, Microarchitecture, Accelerators

## 1 Introduction

The rapid advancement of artificial intelligence, particularly in natural language processing and computer vision, has been driven largely by the success of transformer models [13, 17, 38]. These models have revolutionized machine learning applications, from language translation and text generation [31] to image recognition [29] and autonomous driving [14]. However, the computational demands of transformer models are enormous [37], requiring specialized hardware accelerators to achieve practical performance

and energy efficiency. As these models continue to grow in size and complexity [27], the need for efficient hardware acceleration becomes increasingly critical.

Systolic arrays [30] are specialized hardware architectures that are designed to efficiently perform matrix multiplication by streaming data through a network of processing elements (PEs). In these architectures, data moves only one hop per clock cycle, minimizing hardware data movement overhead and enabling high scalability. Due to their efficiency and scalability, large systolic arrays have been widely adopted in AI accelerators. Notable examples include Google’s TPU [20, 25, 26] (256 $\times$ 256 in TPUv6e and 128 $\times$ 128 prior to v6e) and AWS NeuronCore [9] (128 $\times$ 128).

One of the key operations in transformer models is the *scaled dot-product attention* (SDPA), which is often implemented using the *FlashAttention* [16, 35] algorithm. FlashAttention reduces memory overhead by breaking the  $Q$ ,  $K$ , and  $V$  matrices into small tiles and fusing matrix multiplication with online softmax computation. When mapping FlashAttention to systolic array based accelerators, the matrix multiplication operations can be performed using the systolic array, while the softmax-related operations must be offloaded to a vector unit. To maximize hardware utilization, matrix multiplication and softmax operations from different iterations are often software pipelined to run in parallel. The vector unit must be able to provide sufficient floating-point operations per second (FLOPs/s) to keep up with the systolic array.

However, vector FLOPs/s are typically much lower than matrix multiplication FLOPs/s, resulting in a significant performance bottleneck. For example, AWS NeuronCore-v2 delivers over 90 TFLOPs/s for matrix multiplication, but only 2.3 TFLOPs/s for vector operations [8]. This discrepancy becomes especially severe when the systolic array is large, as the matrix multiplication FLOPs/s scale quadratically with the array size, while vector operation throughput remains limited.

Beyond the imbalance between the matrix multiplication and vector FLOPs, another common challenge in implementing FlashAttention on both systolic arrays and GPUs is register file or SRAM port contention. The concurrent execution of matrix and vector computation leads to port contention when both the systolic array and the vector unit attempt to access the same bank of the register file/SRAM, thereby degrading performance. While existing works like Mosaic [40] and Virgo [28] have aimed to mitigate this contention, they have not fully eliminated it.

The above problems can be addressed if the full FlashAttention algorithm can be executed on a single systolic array, without relying on any external vector unit. In this case, the non-matrix multiplication operations can be performed using the matrix multiplication FLOPs/s of the systolic array, and port contention can be eliminated since all operations are executed on the same array. The key challenges in achieving this are:

- Efficiently executing non-matrix multiplication operations, such as the exp, rowmax, and rowsum functions, using only the systolic array.
- Overlapping different operations efficiently to maximize systolic array utilization.

To address these challenges, we propose **FSA**, an enhanced systolic array architecture that enables the entire FlashAttention algorithm to be executed on a single systolic array, without requiring any external vector unit, based on the following key observations:

- The exp operation in FlashAttention has a limited range of input values, which allows us to implement it using linear interpolation.
- The rowmax and rowsum operations can be implemented using systolic array based reduction, which is a well-studied problem. Since the rows are generated in a streaming fashion on the systolic array, the reduction can be performed on-the-fly.
- After careful study of the dataflow, we observed that the operations of the FlashAttention algorithm can be fully fused and scheduled in a way that allows element-wise operation overlap, enabling the systolic array to perform multiple operations in parallel without waiting for the completion of previous operations.

We further introduce the **SystolicAttention** scheduling algorithm, which maps FlashAttention onto FSA in a way that enables element-wise operation overlap, significantly improving array utilization.

Our key contributions are as follows:

- We propose SystolicAttention, a new scheduling algorithm that enables extensive element-wise overlap of all operations in FlashAttention on systolic arrays, while preserving the original floating-point operation order to maintain numerical stability.
- We design FSA, an enhanced systolic array capable of executing the full FlashAttention algorithm without relying on any additional vector unit. This eliminates port contention entirely and allows ideal performance to be sustained under sufficient memory bandwidth. With our proposed SystolicAttention, FSA achieves  $1.77\times$  and  $4.83\times$  higher FLOPs/s utilization compared to AWS NeuronCore-v2 and TPUv5e, respectively.
- We fully implement FSA in synthesizable RTL and develop a Python programming interface that allows users to write custom FSA kernels. Both the RTL implementation and the Python software stack are open-sourced at <https://github.com/VCA-EPFL/FSA>.

This work not only demonstrates the feasibility of executing the entire FlashAttention algorithm on a single systolic array, but

also opens up new possibilities for systolic array architectures to handle non-linear functions and other complex operations that were previously considered unsuitable for systolic arrays.

## 2 Background and Motivation

In this section, we first briefly introduce systolic arrays and some optimizations that have been proposed based on them. We then present the FlashAttention algorithm and its hardware implementation challenges on systolic array based accelerators.

### 2.1 Matrix Multiplication on Systolic Arrays

To perform matrix multiplication on a systolic array, one of the input matrices or output matrix must be preloaded into the array, while the other input matrix is streamed in and the output matrix is streamed out. When an input matrix is preloaded, the array is termed a *weight-stationary* or *input-stationary systolic array*. For simplicity, this paper uses the term *input-stationary systolic array* to refer to both. If the output matrix is preloaded, the array is known as an *output-stationary systolic array*. Since most deep learning workloads favor input (weight) reuse, most systolic array based accelerators adopt input-stationary architectures.

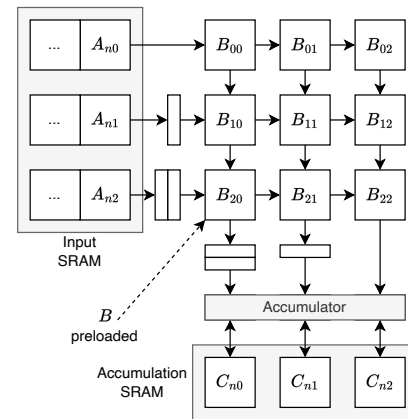


**Figure 1: Computing  $C += AB$  on an input-stationary systolic array.**

An example input-stationary systolic array is shown in Figure 1. It consists of  $N \times N$  processing elements (PEs), where each PE can perform a single floating-point multiply-accumulate (MAC) operation per cycle. One of the input matrices is tiled into shape  $N \times N$  and preloaded into the array, referred to as the *stationary matrix*. The other input matrix is tiled into shape  $N \times M$  and streamed in from input SRAM, referred to as the *moving matrix*. The output matrix is thus tiled into shape  $N \times M$  and streamed out.

Since the input-stationary array does not retain the output matrix internally, output tiles are stored in a small, dedicated accumulation SRAM located at the bottom of the array. An accumulator unit reads values from this accumulation SRAM, combines the newly computed results from the systolic array with existing values, and writes the updated results back. This near-memory accumulation scheme is widely adopted in both open-source accelerators such

as Gemini [18], and commercial products such as AWS Neuron-Core [9].

Preloading the stationary matrix requires  $N$  cycles at the start of computation. To ensure correctness, each row of the moving matrix must be delayed by 0 to  $N - 1$  cycles before entering the array, and each column of the output matrix must be delayed by 0 to  $N - 1$  cycles before being read out. This introduces a total synchronization overhead of  $2N - 1$  cycles. The total computation takes  $M + 3N - 1$  cycles, resulting in an array utilization of  $\frac{M}{M+3N-1}$ . When  $M \gg N$ , this preloading and synchronization overhead is effectively amortized over the duration of the computation.

## 2.2 Systolic Array Optimizations

Several optimizations have been proposed to reduce synchronization overhead in systolic arrays.

Meissa [7] introduces the use of an adder tree for each column in the systolic array to accumulate the results of multiplications. The inputs to the adder tree can be generated in parallel, eliminating the need for synchronization. However, this approach is limited to integer addition, as the adder trees are built using carry-save adders, which are not well-suited for floating-point arithmetic due to the requirements for rounding and exponent alignment.

DIP [2] proposes a diagonal-input dataflow to reduce synchronization latency. However, it requires connecting the leftmost PE to the rightmost PE, violating the one hop per cycle communication property that is fundamental to systolic arrays. This alteration increases hardware wiring complexity and latency.

## 2.3 FlashAttention Algorithm

The FlashAttention algorithm [16, 35] is shown in Algorithm 1, focusing on the computational steps and omitting memory load/store operations for clarity. The exponential function is implemented as  $\exp(x) = 2^{x \log_2 e}$ , following the official open-source FlashAttention implementation, since  $\exp2$  is typically more efficient than  $\exp$  on hardware accelerators.

Matrix multiplications are highlighted in red, while non-matrix operations such as reductions and element wise computations are shown in blue. On GPU-like architectures, matrix multiplications are executed on tensor cores, while non-matrix operations are carried out on SIMT cores. On systolic array based accelerators, matrix multiplications are performed using systolic arrays, and the remaining operations are handled by a separate vector unit or scalar core.

## 2.4 Implementing FlashAttention on Systolic Array Based Accelerators

To implement FlashAttention on current systolic array based accelerators, the result of the first matrix multiplication must be carried out of the systolic array and into a vector unit to perform the softmax-related operations. The intermediate results must then be transferred back into the systolic array to perform the second matrix multiplication.

Lines 15-16 of Algorithm 1 first compute the local output matrix, which is then accumulated into the global output matrix. The accumulation can be fused with the second matrix multiplication

---

### Algorithm 1: FlashAttention-2 and 3 forward pass

---

**Require:** Matrices  $Q, K, V \in \mathbb{R}^{LEN \times d}$

- 1 Divide  $Q$  into  $T_r = \lceil \frac{LEN}{B_r} \rceil$  blocks of size  $B_r \times d$  each, and divide  $K$  and  $V$  into  $T_c = \lceil \frac{LEN}{B_c} \rceil$  blocks of size  $B_c \times d$  each;
- 2 **for**  $1 \leq i \leq T_r$  **do**
- 3     Initialize  $old\_m, old\_l = (-\infty), (0) \in \mathbb{R}^{B_r}$ ;
- 4     Initialize  $old\_O = (0) \in \mathbb{R}^{B_r \times d}$ ;
- 5     **for**  $1 \leq j \leq T_c$  **do**
- 6          $S = Q_i K_j^T \in \mathbb{R}^{B_r \times B_c}$ ;
- 7          $local\_m = \text{rowmax}(S) \in \mathbb{R}^{B_r}$ ;
- 8          $new\_m = \max(local\_m, old\_m) \in \mathbb{R}^{B_r}$ ;
- 9          $a = old\_m - new\_m \in \mathbb{R}^{B_r}$ ;
- 10          $b = \exp(\frac{a}{\sqrt{d}}) = \exp2(\frac{\log_2 e}{\sqrt{d}} a) \in \mathbb{R}^{B_r}$ ;
- 11          $N = S - new\_m \in \mathbb{R}^{B_r \times B_c}$ ;
- 12          $P = \exp(\frac{N}{\sqrt{d}}) = \exp2(\frac{\log_2 e}{\sqrt{d}} N) \in \mathbb{R}^{B_r \times B_c}$ ;
- 13          $local\_l = \text{rowsum}(P) \in \mathbb{R}^{B_r}$ ;
- 14          $new\_l = old\_l \times b + local\_l \in \mathbb{R}^{B_r}$ ;
- 15          $local\_O = PV_j \in \mathbb{R}^{B_r \times d}$ ;
- 16          $new\_O = \text{diag}(b)old\_O + local\_O \in \mathbb{R}^{B_r \times d}$ ;
- 17          $old\_m = new\_m$ ;
- 18          $old\_l = new\_l$ ;
- 19          $old\_O = new\_O$ ;
- 20     **end for**
- 21      $O_i = \text{diag}(old\_l)^{-1}old\_O \in \mathbb{R}^{B_r \times d}$ ;
- 22 **end for**
- 23

---

using the accumulator of the systolic array, so it can be treated as a single matrix multiplication operation.

As explained in Section 2.1, additional synchronization and preloading overheads are incurred when moving data in and out of the systolic array. To maximize systolic array utilization, the tile size must be large enough to amortize these overheads. However, a larger tile size also leads to a greater imbalance between the matrix multiplication and vector FLOPs, as well as increased SRAM requirements for storing intermediate results.

Consequently, a significant amount of software tuning is required in addition to software pipelining, and it remains challenging to achieve high performance when implementing FlashAttention on systolic array based accelerators.

## 3 SystolicAttention Scheduling Algorithm

The goal of our design is to execute the FlashAttention algorithm on a single systolic array, thereby improving the FLOPs/s for the non-matrix multiplication operations and eliminating the need for an external vector unit.

To enable the execution of non-matrix multiplication operations of the FlashAttention algorithm on a single systolic array, we add a row of comparison units at the top of the array to perform the on-the-fly rowmax operation. Additionally, we introduce a *Split* unit in each PE to implement the  $\exp$  operation. To allow the rowmax,

exp, and rowsum operations to overlap with matrix multiplication, we incorporate an upward data path in the systolic array.

In this section, we first provide an overview of the enhanced systolic array microarchitecture, FSA, that we propose to accelerate the FlashAttention algorithm. We then describe how the non-matrix operations in FlashAttention can be executed using FSA. Finally, we demonstrate how to extensively overlap different computations within FSA in a systolic manner using our proposed SystolicAttention scheduling algorithm.

### 3.1 FSA Overview

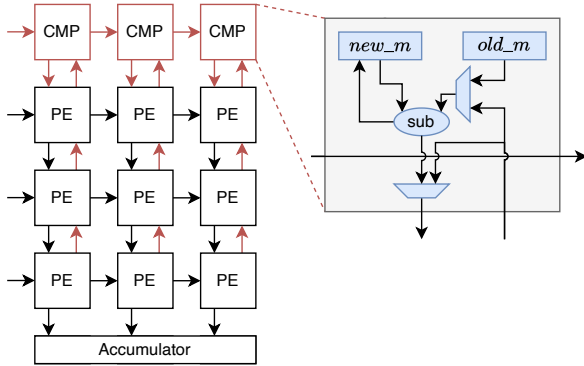


Figure 2: FSA’s modifications to standard systolic array.

FSA’s three modifications to the standard systolic array are highlighted in red in Figure 2:

**A row of comparison units:** We add a row of comparison units at the top of the array to compute the maximum value of each column of the systolic array output on the fly. Each comparison unit consists of a floating-point adder and two registers. One register, *old\_m* holds the maximum value from the previous iteration. The other register, *new\_m*, stores the temporary maximum value of the current iteration. The value of *new\_m* is updated based on the comparison result, performed by subtracting the two values using the floating-point adder. The difference between the inputs can also be generated using the floating point adder, which is useful to compute Line 9 of Algorithm 1.

**A Split unit in each PE:** We add a *Split* unit to each PE to split the input floating-point number into its integer and fractional parts. This is used to implement the exp2 operation in a piecewise linear fashion.

**Upward data path:** Standard systolic arrays only support propagation of partial sums from matrix multiplication in one direction. We add an additional data path to propagate the partial sums in the opposite direction. This allows computation to begin from either the top or bottom of the array.

### 3.2 rowmax on FSA

Figure 3 illustrates the fused matrix multiplication and rowmax computation, which corresponds to Lines 6–8 of Algorithm 1. The matrix multiplication  $S = Q_i K_j^T$  is performed in the systolic array along the upward data path, such that the **rows** of  $S$  become the **columns** of the systolic array and exit the array from the top.

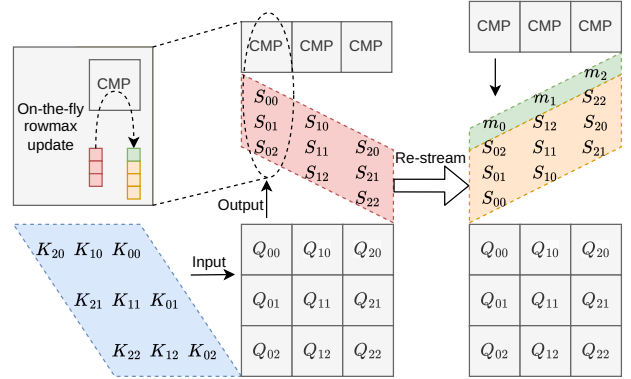


Figure 3: On-the-fly rowmax generation.

The rowmax operation is executed in the comparison units concurrently with the generation of each row of  $S$ . As the rows of  $S$  are produced, they are re-streamed from the top of the array back down through the comparison units. By the time the maximum value of each row is computed,  $S$  is already resident in the systolic array.

Consequently, the subtraction operation  $N = S - new\_m$  from Line 11 of Algorithm 1 can be performed immediately. This is achieved by streaming constant ones from the left of the array as the multiplicand, and streaming *new\_m* from the top of the array as the addend.

### 3.3 exp and exp2 on FSA

After the rowmax and subtraction operations, an element-wise exponential function must be applied to the matrix  $N$ , as shown in Line 12 of Algorithm 1:

$$P = \exp\left(\frac{N}{\sqrt{d}}\right) = \exp2\left(\frac{\log_2 e}{\sqrt{d}} \cdot N\right).$$

The exp function is implemented using exp2, which is typically more efficient on hardware accelerators [23]. The constant multiplication  $\frac{\log_2 e}{\sqrt{d}} \cdot N$  can be computed by streaming the constant  $\frac{\log_2 e}{\sqrt{d}}$  from the left of the array as the multiplicand, since the matrix  $N$  is already resident in the systolic array after the subtraction operation. For the element-wise exp2 operation, we use a piecewise linear interpolation to approximate the function [36].

A floating-point number  $x$  can be split into its integer and fractional parts:  $x = x_i + x_f$ , where  $x_i$  is the integer part and  $x_f$  is the fractional part [1]. This leads to the identity:

$$\exp2(x) = 2^{x_i + x_f} = 2^{x_i} \cdot 2^{x_f}.$$

Since  $N = S - \text{rowmax}(S)$ , all elements in  $N$  are less than or equal to zero. This implies  $x_f \in (-1, 0]$ , and therefore  $2^{x_f} \in (0.5, 1]$ . Given this limited range for  $x_f$ , we find that an 8-piece uniform piecewise linear interpolation is sufficient to achieve a relative error around  $10^{-3}$  to  $10^{-2}$  in the final FlashAttention results:

$$\exp2(x) \approx 2^{x_i} \cdot \left(\text{slope}_k \cdot x_f + \text{intercept}_k\right), \quad k \in [0, 8).$$

As shown in Figure 4, the piecewise linear interpolation for  $x_f$  can be implemented by reusing the MAC units in the systolic array.

A simple *Split* unit is added to separate the input  $x$  into its integer and fractional parts. The *Split* unit extracts  $x_i$  and  $x_f$  by shifting the mantissa bits to align the exponent to zero. The term  $2^{x_i}$  affects only the exponent bits in the final result, effectively increasing the exponent by  $x_i$ .

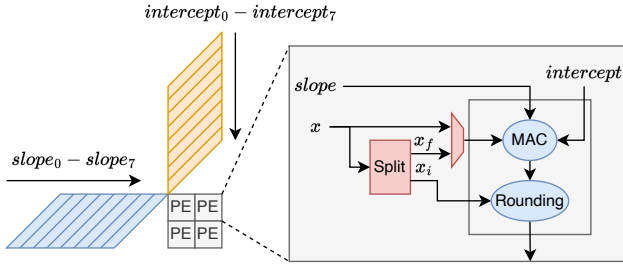


Figure 4:  $\exp 2$  using piecewise linear interpolation.

To avoid the need for storing the piecewise linear interpolation coefficients in the systolic array, we stream the  $slope_k$  and  $intercept_k$  values from the left and top of the array, respectively. We further observe that all intercepts lie in the range  $(0.5, 1]$ , so their exponent can only be 0 or  $-1$ . The MSBs of their exponents can be used to encode the interpolation index  $k$ . This enables each PE to update its register based on  $k$  without requiring additional control signals.

### 3.4 rowsum on FSA

Benefiting from the in-place  $\exp$  computation of  $P = \exp\left(\frac{N}{\sqrt{d}}\right)$  in the systolic array, the rowsum operation can begin as soon as the top-left element of  $P$  is produced.

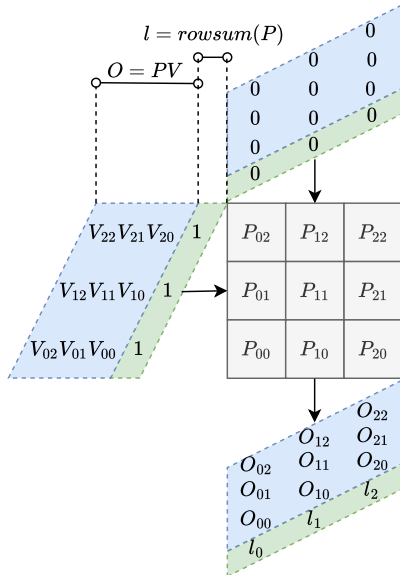


Figure 5: rowsum using systolic array.

As shown in Figure 5, the rowsum of  $P$  can be computed by streaming constant ones from the left of the array as the multiplicand, and streaming zeros from the top of the array as the addend. The second matrix multiplication,  $O = P \cdot V$  can then be performed in the systolic array along the downward data path, starting one cycle after the rowsum operation begins. Once the rowsum  $local\_l$  and the output  $local\_O$  exit the array from the bottom, they are accumulated with the previous values  $old\_l$  and  $old\_O$  in the accumulator, and the results update  $new\_l$  and  $new\_O$  in the accumulation SRAM, respectively.

### 3.5 Overlapping Computations with SystolicAttention

So far, we have introduced the key operations required to perform FlashAttention within a systolic array, including rowmax,  $\exp 2$ , and rowsum. We now describe how these operations can be overlapped in a systolic fashion to maximize efficiency.

Each iteration of the FlashAttention algorithm involves two matrix multiplications. To avoid costly data movement between the systolic array and external SRAM, we structure computation on an  $N\_ROWS \times N\_COLS$  systolic array by selecting tile sizes  $B_r = N\_COLS$  and  $B_c = N\_ROWS = d$ . This allows the output of the first matrix multiplication,  $S = Q_i K_j^T$ , to be directly re-streamed into the array as input for the second matrix multiplication.

During the first matrix multiplication, the head dimension  $d$  of both  $Q$  and  $K$  is mapped to  $N\_ROWS$ , while the sequence length  $B_r$  of  $Q$  is mapped to  $N\_COLS$ . After computing  $S$ , we re-stream it from the top of the array, mapping the  $B_c$  dimension of  $S$  to  $N\_ROWS$ . A sequence of element-wise operations is then performed in-place cycle by cycle to transform  $S$  into  $N$  and then into  $P$ .

For the second matrix multiplication,  $O = P \cdot V$ , the  $B_c$  dimension of  $V$  is mapped to  $N\_ROWS$  and contracted with the stationary matrix  $P$  inside the systolic array.

We use the upward data path for the first matrix multiplication, such that the elements of  $P$  are generated from the top left to the bottom right of the array. Then, by leveraging the downward data path, we can immediately begin the second matrix multiplication once the top-left element of  $P$  is available.

Figure 6 illustrates the execution of the entire inner loop. The fifth operation,  $a = old\_m - new\_m$ , passes down the difference between the previous and current maximum values from comparison units to the accumulator. This operation runs in parallel with the constant multiplication  $\frac{\log_2 e}{\sqrt{d}} \cdot N$ , as the downward data path is idle during the in-place constant multiplication.

Overall, each iteration takes only  $2 \cdot N\_COLS + 3 \cdot N\_ROWS + 10$  cycles, meaning that on an  $N \times N$  systolic array, it takes just  $5N + 10$  cycles to process a  $N \times N$  FlashAttention tile. By contrast, on a naive  $N \times N$  systolic array, the two independent matrix multiplications alone may require up to  $8N - 2$  cycles due to preloading and synchronization overheads discussed in Section 2.1.

The re-scaling operation in Line 21 of Algorithm 1 is only performed once per outer loop. It is executed using the accumulator after the second matrix multiplication completes. In our implementation, this re-scaling step takes  $2N + 20$  cycles, which is negligible compared to the inner loop execution time.

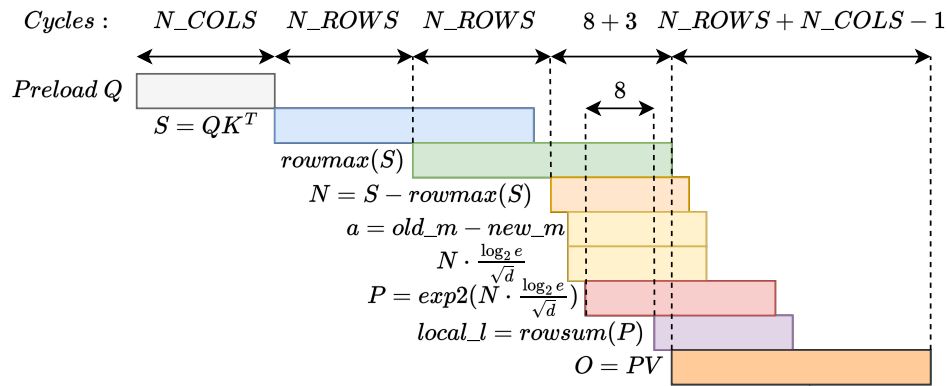


Figure 6: Overlapped computations of the FlashAttention inner loop in the systolic array.

## 4 FSA Microarchitecture

FSA modifies the standard systolic array architecture to support the SystolicAttention algorithm. To validate its feasibility and quantify the associated hardware overhead, we implement FSA in RTL and design a minimal yet flexible instruction set capable of executing the full FlashAttention.

The RTL design is implemented in Chisel HDL [11] and built using the Chipyard [3–5, 15] framework for system-on-chip (SoC) construction. Unlike prior efforts such as Gemmini [18], which focus on flexible design space exploration, our goal is to deliver a concrete and complete implementation of FSA to validate both the practicality of the SystolicAttention algorithm and its hardware cost.

This section provides an overview of the FSA microarchitecture, details the instruction set design that simplifies the hardware implementation, and describes the systolic array controller that orchestrates the execution of the SystolicAttention algorithm.

### 4.1 Microarchitecture Overview

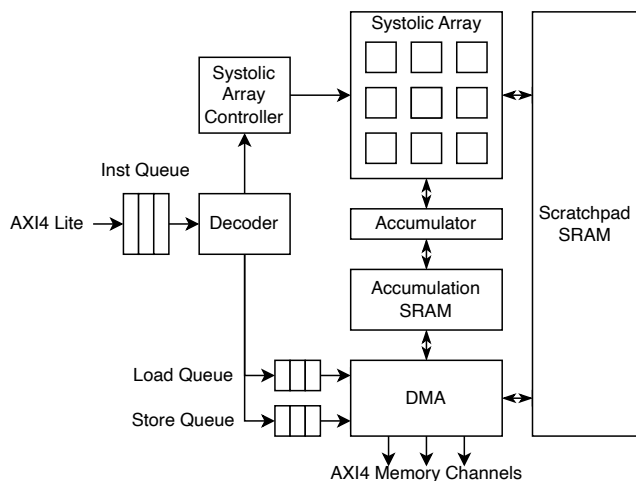


Figure 7: FSA microarchitecture.

An overview of the FSA microarchitecture is shown in Figure 7. FSA receives instructions via an AXI4-Lite interface and accesses backing memory through a configurable number of AXI4 memory interfaces.

The instruction decoder classifies instructions into three types: *load*, *store*, and *compute*. Instructions of different classes are executed asynchronously, while instructions of the same class execute in order but may be interleaved.

The systolic array controller issues compute instructions once the required data has been loaded into SRAM. To simplify control logic, FSA prioritizes SRAM access over compute operations, making the latency of compute instructions fully deterministic once issued. This design allows the controller to statically schedule control signals based on the known execution cycle of each instruction.

The DMA engine follows an iDMA-style interface [12] and supports 2D data transfers. Each DMA instruction can specify source and destination addresses in SRAM and backing memory, along with the transfer size and stride.

When multiple AXI4 channels are available, the DMA engine automatically partitions the transfer into parallel AXI4 transactions, maximizing memory bandwidth utilization.

### 4.2 FSA Instruction Set

To enable fine-grained overlap between various FlashAttention operations, the systolic array in FSA requires more sophisticated control logic than standard systolic arrays. The primary design goal of the FSA instruction set is to ensure that compute instructions execute in a fully deterministic manner, independent of memory access latency. This simplification greatly reduces control complexity.

To achieve this, we define five compute instructions based on their SRAM data dependencies, as illustrated in Figure 8. The FlashAttention inner loop is divided into three phases:

- **Load Stationary:** Preload  $Q$  into the systolic array.
- **Attn Score:** Perform the first matrix multiplication using  $Q$  and  $K$ , fused with element-wise online softmax to compute the  $P$  matrix in-place within the systolic array. The log of the exponent sum for  $P$  is also calculated during this step.
- **Attn Value:** Perform the second matrix multiplication using  $V$  and  $P$ .

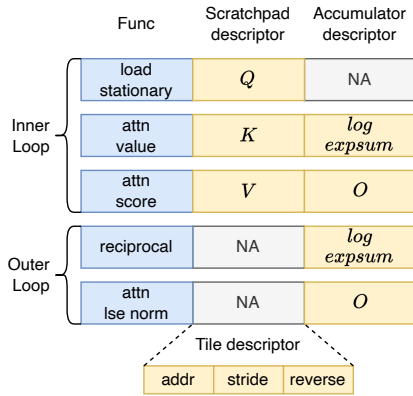


Figure 8: FSA compute instructions.

The FlashAttention outer loop is divided into two additional phases:

- **Reciprocal:** Load the log exponent sum of  $P$  from the accumulation SRAM and compute its reciprocal. The result is stored in the accumulator as a scaling factor for the next phase.
- **Attn LSE Norm:** Load the output matrix  $O$  from the accumulator and apply the reciprocal scaling factor.

Each compute instruction reads one input tile from SRAM and writes one output tile to the accumulator SRAM. This one-tile-in, one-tile-out design ensures that compute instructions can be executed as soon as their corresponding SRAM tile is ready—without waiting on other tiles to be loaded or processed.

DMA instructions follow a similar structure to compute instructions, consisting of one memory tile descriptor and one SRAM tile descriptor. However, they use wider bit fields to support large memory address spaces.

### 4.3 Systolic Array Controller

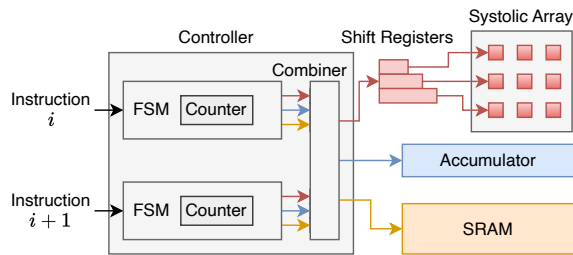


Figure 9: FSA systolic array controller.

The microarchitecture of the FSA systolic array controller is illustrated in Figure 9. The controller comprises two identical counter-based finite state machines (FSMs), each responsible for generating control signals for a compute instruction.

Control signals are categorized into three types:

- **PE Control Signals:** Define the operations to be performed within the PEs of the systolic array.

- **Accumulator Control Signals:** Specify the actions performed in the accumulator.
- **SRAM Control Signals:** Govern the read and write operations to SRAM required for executing the compute instruction.

Because compute instruction execution is fully deterministic, the counter is initialized at the start of each compute instruction, incremented every cycle, and reset to zero upon completion. As a result, the FSMs can generate control signals solely based on the instruction type and the current counter value.

To simplify control logic development, we implemented a domain specific language (DSL) on top of Chisel and Scala. This DSL allows designers to specify which control signals should be scheduled at each cycle. The control logic is then automatically synthesized from the DSL specification.

The dual-FSM architecture enables overlapping execution of two compute instructions. For example, the *Attn Value* instruction can begin as soon as the *Attn Score* instruction produces the first element of the  $P$  matrix. A combiner unit merges the control signals from both FSMs, ensuring that signals are emitted in the correct order and that conflicts are avoided.

## 5 FSA Kernel Programming Model

The AWS Neuron Kernel Interface (NKI) [10] provides an expressive Python interface that allows users to write custom kernels for AWS Neuron devices. It offers instruction-level control with the convenience of Python APIs.

Inspired by AWS NKI, FSA provides a similar, simplified Python library for writing custom FSA kernels. The library consists of three main components: type-safe tensors, a Python API for the FSA instruction set, and a lightweight JIT compiler.

### 5.1 Type-Safe Tensors

The FSA Python library implements a PyTorch-like [6, 32] tensor abstraction for representing multi-dimensional arrays. Because the memory hierarchy is fully user-managed, tensors can be allocated in one of three memory spaces: main memory, scratchpad SRAM, or accumulation SRAM. Accordingly, we define three tensor types:

- **MTile** – for main memory tensors,
- **STile** – for scratchpad SRAM tensors,
- **ATile** – for accumulation SRAM tensors.

All tensor types support a subset of the PyTorch API, including shape, dtype, split, and reverse. By explicitly distinguishing tensor types, users can write custom kernel functions that clearly declare the expected input and output tensor memory scopes.

### 5.2 Python API for FSA Instructions

Each FSA instruction is exposed through a corresponding Python API. These APIs are designed to be type-safe, ensuring correct usage of tensor types. The complete set of supported APIs is shown in Listing 1.

Listing 1: FSA Python instructions.

```
# DMA Instructions
def store_tile(src: ATile, dst: MTile, ...)
def load_tile(src: MTile, dst: STile, ...)
```

```
# Compute Instructions
def load_stationary(tile: STile, ...)
def attn_score(K: STile, l: ATile, ...)
def attn_value(V: STile, o: ATile, ...)
def reciprocal(l: ATile, ...)
def attn_lse_norm(o: ATile, ...)
```

Internally, these functions construct hardware instructions using the metadata of the input tensors—such as shape, stride, and data type. This abstraction allows users to write high-level kernels without managing low-level hardware details.

### 5.3 JIT Kernel Compiler

We provide a lightweight JIT compiler that compiles decorated Python functions into FSA binary programs. These programs consist of a sequence of binary instructions that can be submitted to the device’s instruction queue for execution.

The FlashAttention kernel implemented in FSA using the JIT compiler is shown in Listing 2.

**Listing 2: FSA FlashAttention kernel.**

```
import fsa as F

@F.kernel(device="verilator_sim")
def attention(Q: MTile, K: MTile, Vt: MTile) -> MTile:
    # allocate output tensor
    Ot: MTile = F.alloc_mem(...)
    # split large tensors into tiles
    Ot_MTiles = Ot.split(br, dim=-1) # [d, br]
    Q_MTiles = Q.split(br, dim=-2) # [br, d]
    K_MTiles = K.split(bc, dim=-2) # [br, d]
    Vt_MTiles = Vt.split(bc, dim=-1) # [d, bc]
    # double buffering for Q, K, Vt
    K_STiles = (F.alloc_spad(...), F.alloc_spad(...))
    Vt_STiles = (F.alloc_spad(...), F.alloc_spad(...))
    # allocate space for accumulation results
    log_expsum = F.alloc_accum(...) # [1, br]
    Ot_ATile = F.alloc_accum(...) # [d, br]

    for i, Q_i in enumerate(Q_MTiles):
        F.load_tile(Q_i, Q_STiles[i %
        for j, (K_j, Vt_j) in enumerate(zip(K_MTiles,
            Vt_MTiles)):
            F.load_stationary(Q_STiles[i %
            F.load_tile(K_j, K_STiles[j %
            F.attn_score(K_STiles[j %
            F.load_tile(Vt_j, Vt_STiles[j %
            F.attn_value(Vt_STiles[j %
            F.reciprocal(log_expsum)
            F.attn_lse_norm(Ot_ATile)
            F.store_tile(Ot_ATile, Ot_MTiles[i])

    # Run simulation and return result
    Ot = attention(Q, K, Vt)
    O = Ot.to_numpy().T # Host-side transpose
```

The JIT compiler processes Python functions decorated with `@F.kernel`. The decorator also specifies the target device (e.g., a Verilator-based simulator [39]), and handles device-host communication automatically.

In the example above, the host loads input tensors into device memory using DRAMSim2 [34], dispatches the compiled instructions to the FSA device, and retrieves the output tensors upon completion. The output is then converted to NumPy [22] arrays for post-processing.

Since FSA currently does not support matrix transpose operations in hardware, the input matrix  $V$  must be transposed in advance, and the resulting output matrix  $O$  is returned in transposed form.

## 6 Evaluation

### 6.1 FlashAttention Performance

We compare the FlashAttention performance of FSA with state-of-the-art commercial systolic-array-based accelerators, including Google’s TPUv5e [21] and AWS NeuronCore-v2 [8]. We select TPUv5e because it has the same systolic array size,  $128 \times 128$ , as AWS NeuronCore-v2. For fairness, we also configure FSA with a  $128 \times 128$  systolic array. All accelerators use 16-bit floating point activation and 32-bit accumulation.

The accelerator configurations used for evaluation are summarized in Table 1. We evaluate the FlashAttention forward pass performance of a single attention head on all three accelerators, using a head dimension of 128, without causal masking, and with sequence lengths ranging from 2048 to 16384.

To clarify, we use the term *FLOPs* to denote the number of floating-point operations, and *FLOPs/s* to indicate the number of floating-point operations performed per second. Although all accelerators share the same systolic array size, their absolute performance still varies due to differences in clock frequency, which in turn depend on the specific node technology employed. Therefore, we simulate FSA at 1 GHz, a target that is easily achievable in 16 nm technology, as discussed in Section 6.3, and compare matrix multiplication *FLOPs/s* utilization rather than wall-clock execution time.

**Table 1: Accelerator configurations used for evaluation.**

Accelerator	TPUv5e	Neuron-v2	FSA
Systolic array size	$128 \times 128$	$128 \times 128$	$128 \times 128$
Number of arrays	4	1	1
TFLOPs/s (MAC only)	196.6	91.75	32.77
Frequency	1.5GHz <sup>1</sup>	2.8GHz	1GHz
Memory Bandwidth	819GB/s	820GB/s	512GB/s
Scratchpad SRAM	48MiB	24MiB	192KiB <sup>2</sup>
Accumulation SRAM		2MiB	64KiB
Require Vector Unit?	<b>Yes</b>	<b>Yes</b>	<b>No</b>

<sup>1</sup> The clock frequency of TPUv5e is inferred from its reported performance using the formula:  $\text{freq}_{\text{GHz}} = \frac{\text{TFLOPs} \cdot 10^{12}}{2 \cdot 128 \cdot 128 \cdot 10^9}$ .

<sup>2</sup> Since FSA operates on  $128 \times 128$  tiles and only targets FlashAttention operations in this experiment, 192 KiB of SRAM is sufficient to support the algorithm using double buffering.

The number of floating-point operations in a FlashAttention inner loop is given by:

$$\text{FLOPs/InnerLoop} = 2 \times 2 \times B_r \times B_c \times d$$

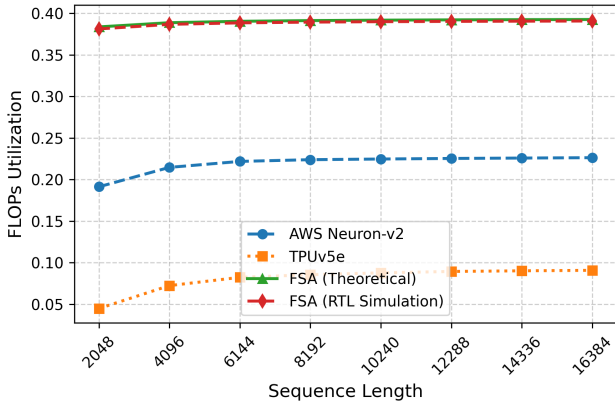


**Figure 10: FlashAttention FLOPs/s utilization of FSA compared to TPUv5e and AWS NeuronCore-v2.**

where each matrix multiplication contributes  $2 \times B_r \times B_c \times d$ . The total number of operations is:

$$\text{FLOPs} = \frac{\text{SeqLen}}{B_r} \times \text{FLOPs/InnerLoop} \times \frac{\text{SeqLen}}{B_c} = 4 \times \text{SeqLen}^2 \times d$$

This matches the formula used in FlashAttention [16].

We calculate the achieved FLOPs/s on each accelerator as follows:

$$\text{Achieved FLOPs/s} = \frac{\text{Total FLOPs}}{\text{Execution Time}}$$

and the FLOPs/s utilization as:

$$\text{FLOPs/s Utilization} = \frac{\text{Achieved FLOPs/s}}{\text{Peak FLOPs/s}}$$

We use the official FlashAttention kernel implementations for the two commercial accelerators, which are optimized for their respective architectures:

- `jax.pallas.ops.tpu.flash_attention` for TPUv5e [24].
- `neuronxcc.nki.kernels.attention.flash_fwd` for the AWS NeuronCore-v2 [10].

The experimental results are shown in Figure 10. Benefiting from intensively overlapped computations, FSA achieves average FLOPs/s utilization that is 1.77 times and 4.83 times higher compared to TPUv5e and AWS NeuronCore-v2, respectively. Moreover, the results confirm that our RTL implementation of FSA closely aligns with the theoretical performance outlined in Section 3.5, validating the correctness of our RTL design.

## 6.2 Accuracy Analysis

The SystolicAttention produces mathematically equivalent results to standard attention and preserves the order of floating-point operations. However, due to the piecewise linear interpolation used for the  $\exp_2$  computation, the final results may differ slightly from those generated by commercial accelerators.

In this section, we first analyze the accuracy of the piecewise linear approximation of the single  $\exp_2$  function. We then assess its overall impact on the final attention results.

**6.2.1 Error Analysis of Piecewise Linear Approximation.** Since the input to the  $\exp_2$  function in the FlashAttention is always negative, we exhaustively evaluate the piecewise linear approximation over all negative normal fp16 values. We exclude subnormal values, as they are typically flushed to zero in most accelerators [19].

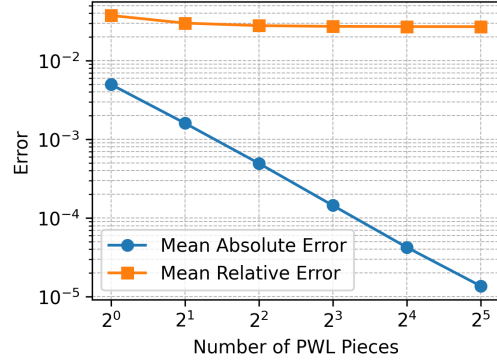


**Figure 11:  $\exp_2$  piecewise linear interpolation error analysis.**

Figure 11 shows the mean absolute error (MAE) and mean relative error (MRE) of the piecewise linear approximation of the  $\exp_2$  function, plotted against the number of segments used in the approximation.

The MAE decreases significantly as the number of segments increases, while the MRE remains relatively stable. This occurs because the breakpoints in the approximation are uniformly spaced, whereas the fp16 representation is logarithmic in nature, making relative error more sensitive for values close to zero.

We choose to use 8 segments in our FSA implementation, which achieves a MAE of 0.00014 and an MRE of 0.02728. Although non-uniformly spaced breakpoints could further reduce the MRE, we leave this exploration for future work.

**6.2.2 Overall FlashAttention Accuracy.** To evaluate the accuracy of the FlashAttention attention on FSA, we compare it against `torch.nn.functional.scaled_dot_product_attention` in PyTorch [6]. We use the same head dimension and sequence lengths as in the performance evaluation. The input matrices  $Q, K, V$  are randomly generated with a normal distribution in the range of  $[0, 1]$ .

The overall FlashAttention accuracy results are shown in Table 2. The MAE lies in the range of  $10^{-4}$  to  $10^{-3}$ , while the MRE is around  $10^{-3}$  to  $10^{-2}$ . These results indicate that the piecewise linear approximation of the  $\exp_2$  function has a negligible impact on the final attention results.

## 6.3 FSA Area Overhead

The area overhead of FSA arises from the following additional components:

- The upward data path, in addition to the standard downward path, enabling partial sums to propagate in both directions.
- A top row of *CMP* units, responsible for identifying the maximum value in each systolic array column.

**Table 2: Mean absolute error (MAE), mean squared error (MSE), and mean relative error (MRE) of the FlashAttention results on FSA.**

SeqLen	MAE	MSE	MRE
2048	1.269e-03	3.219e-04	2.532e-03
4096	3.022e-04	6.302e-05	6.043e-04
6144	8.742e-05	1.142e-08	1.747e-04
8192	1.234e-03	2.914e-04	2.470e-03
10240	9.175e-05	1.246e-08	1.832e-04
12288	9.071e-05	1.222e-08	1.811e-04
14336	2.563e-03	6.500e-04	5.125e-03
16384	1.021e-03	2.324e-04	2.041e-03

- A *Split* unit within each processing element (PE), which separates input values into integer and fractional parts for the  $\exp_2$  operation.

To evaluate the area overhead, we synthesize the systolic array portion of FSA, excluding SRAMs and DMA, at 1 GHz using a 16 nm commercial process. The resulting area breakdown is shown in Table 3.

**Table 3: FSA area breakdown.**

Group	Component	Area (%)	Area ( $\mu\text{m}^2$ )
Standard	PEs (excluding Split units)	84.10	16629356
	Other logic	5.63	1111842
	<i>Total</i>	89.73	17741199
FSA additional	Upward data path	4.83	956556
	Split units	4.78	945322
	CMP units	0.65	128012
	<i>Total</i>	10.26	2029891

As shown in Table 3, the standard systolic array occupies 89.73% of the total area, while FSA’s additional components contribute 10.26%. The dominant sources of overhead are the upward data path and the *Split* units, which account for 4.83% and 4.78% of the total area, respectively. This is due to their replication across all PEs in the  $128 \times 128$  array. In contrast, the *CMP* units contribute only 0.65%, as they are instantiated solely in the top row of the array.

## 7 Discussion

### 7.1 Computing Non-Linear Functions on Systolic Arrays

We observe that the piecewise linear approximation of the  $\exp_2$  function on systolic arrays has strong potential to generalize to other non-linear functions.

In general, if a non-linear function can be segmented into multiple intervals, each well-approximated by a linear function, then piecewise linear approximation can be applied. This enables the computation of non-linear functions using the high-throughput FLOPs/s capacity of systolic arrays—substantially exceeding that of traditional vector units.

### 7.2 Necessity of a Vector Unit

While FSA is capable of executing FlashAttention entirely on the systolic array without relying on a vector unit, a vector or special function unit (SFU) is still necessary in a full accelerator system to support activation functions outside of FlashAttention.

However, because FSA offloads all attention-related computation from the vector unit, the overall vector FLOPs/s requirement may be significantly reduced.

### 7.3 FSA Variant: Area-Optimized Design

This paper focuses on the most performant FSA variant, which uses both upward and downward data flow to maximize throughput.

However, during development, we also explored a simpler variant with a single data flow direction, similar to a standard systolic array. This configuration still supports the SystolicAttention algorithm, but introduces additional latency: the second matrix multiplication ( $O = PV$ ) cannot begin immediately after the first elements of  $P$  are computed and must wait for the entire  $P$  matrix.

This results in the inner loop latency increasing from  $5N + 10$  to  $6N + 10$  cycles. Despite this, this area-optimized design would still deliver higher FLOPs/s utilization than commercial accelerators.

### 7.4 Limitations of FSA

Although FSA delivers high FLOPs/s utilization for FlashAttention, it is not well-suited for the decoding phase of LLM inference.

FSA is ideal for the (1) LLM training and (2) prefill phase of LLM inference, where the query matrix  $Q$  has a long sequence length, making the attention computation compute-intensive [33]. In this case, the high FLOPs/s throughput of FSA effectively accelerates the workload.

In contrast, during the decoding phase, the query  $Q$  has a sequence length of 1, making the computation memory-bound. Moreover, since FSA operates on  $128 \times 128$  tiles,  $Q$  must be padded to fit this shape, resulting in substantial wasted computation and inefficient resource usage.

## 8 Conclusion

We have presented FSA, an enhanced systolic array architecture that enables complete FlashAttention computation within a single systolic array. At the core of our approach is the SystolicAttention algorithm, which achieves extensive element-wise overlap of all FlashAttention operations through careful scheduling and static data flow management.

The experimental results validate our approach, showing significant improvements in FLOPs/s utilization compared to state-of-the-art commercial accelerators while maintaining high accuracy and requiring minimal on-chip memory.

Beyond demonstrating the feasibility of executing complete FlashAttention computation on a single systolic array, our work establishes new possibilities for systolic array architectures to efficiently handle non-linear functions and complex operations that were previously deemed unsuitable for such architectures.

## References

- [1] 2019. IEEE Standard for Floating-Point Arithmetic. *IEEE Std 754-2019 (Revision of IEEE 754-2008)* (2019), 1–84. doi:10.1109/IEEESTD.2019.8766229

- [2] Ahmed J. Abdelmaksoud, Shady Agwa, and Themis Prodromakis. 2024. DiP: A Scalable, Energy-Efficient Systolic Array for Matrix Multiplication Acceleration. arXiv:2412.09709 [cs.AR] <https://arxiv.org/abs/2412.09709>
- [3] Alon Amid, David Biancolin, Abraham Gonzalez, Daniel Grubb, Sagar Karandikar, Harrison Liew, Albert Magyar, Howard Mao, Albert Ou, Nathan Pemberton, Paul Rigge, Colin Schmidt, John Wright, Jerry Zhao, Jonathan Bachrach, Sophia Shao, Borivoje Nikolić, and Krste Asanović. 2020. Invited: Chipyard - An Integrated SoC Research and Implementation Environment. In *2020 57th ACM/IEEE Design Automation Conference (DAC)*. 1–6. doi:10.1109/DAC18072.2020.9218756
- [4] Alon Amid, David Biancolin, Abraham Gonzalez, Daniel Grubb, Sagar Karandikar, Harrison Liew, Albert Magyar, Howard Mao, Albert Ou, Nathan Pemberton, Paul Rigge, Colin Schmidt, John Wright, Jerry Zhao, Yakun Sophia Shao, Krste Asanović, and Borivoje Nikolić. 2020. Chipyard: Integrated Design, Simulation, and Implementation Framework for Custom SoCs. *IEEE Micro* 40, 4 (2020), 10–21. doi:10.1109/MM.2020.2996616
- [5] Alon Amid, Albert Ou, Krste Asanović, Yakun Sophia Shao, and Borivoje Nikolić. 2021. Vertically Integrated Computing Labs Using Open-Source Hardware Generators and Cloud-Hosted FPGAs. In *2021 IEEE International Symposium on Circuits and Systems (ISCAS)*. 1–5. doi:10.1109/ISCAS51556.2021.9401515
- [6] Jason Ansel, Edward Yang, Horace He, Natalia Gimelshein, Animesh Jain, Michael Voznesensky, Bin Bao, Peter Bell, David Beard, Evgeni Burovski, Geeta Chauhan, Anjali Chourdia, Will Constable, Alban Desmaison, Zachary DeVito, Elias Ellison, Will Feng, Jiong Gong, Michael Gschwind, Brian Hirsh, Sherlock Huang, Kshiteej Kalambarkar, Laurent Kirsch, Michael Lazos, Mario Lezcano, Yanbo Liang, Jason Liang, Yinghai Lu, C. K. Luk, Bert Maher, Yunjie Pan, Christian Puhresch, Matthias Reso, Mark Saroufim, Marcos Yukio Siraichi, Helen Suk, Shunting Zhang, Michael Suo, Phil Tillet, Xu Zhao, Eikan Wang, Keren Zhou, Richard Zou, Xiaodong Wang, Ajit Mathews, William Wen, Gregory Chanan, Peng Wu, and Soumith Chintala. 2024. PyTorch 2: Faster Machine Learning Through Dynamic Python Bytecode Transformation and Graph Compilation. In *Proceedings of the 29th ACM International Conference on Architectural Support for Programming Languages and Operating Systems, Volume 2 (La Jolla, CA, USA) (ASPLOS '24)*. Association for Computing Machinery, New York, NY, USA, 929–947. doi:10.1145/3620665.3640366
- [7] Bahar Asgari, Ramyad Hadidi, and Hyesoon Kim. 2020. MEISSA: Multiplying Matrices Efficiently in a Scalable Systolic Architecture. In *2020 IEEE 38th International Conference on Computer Design (ICCD)*. 130–137. doi:10.1109/ICCD50377.2020.00036
- [8] AWS Neuron Documentation. 2024. *NeuronCore-v2 Architecture*. <https://awsdocs-neuron.readthedocs-hosted.com/en/latest/general/arch/neuron-hardware/neuron-core-v2.html#neuroncores-v2-arch> Accessed: 2025-06-15.
- [9] AWS Neuron Documentation. 2024. *Trainium/Inferentia2 Architecture Guide for NKI*. [https://awsdocs-neuron.readthedocs-hosted.com/en/latest/general/nki/arch/trainium\\_inferentia2\\_arch.html#trainium-inferentia2-arch](https://awsdocs-neuron.readthedocs-hosted.com/en/latest/general/nki/arch/trainium_inferentia2_arch.html#trainium-inferentia2-arch) Accessed: 2025-06-15.
- [10] AWS Neuron Team. 2025. AWS Neuron NKI Samples. <https://github.com/aws-neuron/nki-samples>. Accessed: 2025-06-30.
- [11] Jonathan Bachrach, Huy Vo, Brian Richards, Yunsup Lee, Andrew Waterman, Rimas Aviziemis, John Wawrzynek, and Krste Asanović. 2012. Chisel: constructing hardware in a Scala embedded language. In *Proceedings of the 49th Annual Design Automation Conference (San Francisco, California) (DAC '12)*. Association for Computing Machinery, New York, NY, USA, 1216–1225. doi:10.1145/2228360.2228584
- [12] Thomas Benz, Michael Rogenmoser, Paul Scheffler, Samuel Riedel, Alessandro Ottaviano, Andreas Kurth, Torsten Hoefler, and Luca Benini. 2024-01. A High-performance, Energy-efficient Modular DMA Engine Architecture. *IEEE Trans. Comput.* 73, 1 (2024-01), 263 – 277. doi:10.3929/ethz-b-000641982
- [13] Tom B. Brown, Benjamin Mann, Nick Ryder, Melanie Subbiah, Jared Kaplan, Prafulla Dhariwal, Arvind Neelakantan, Pranav Shyam, Girish Sastry, Amanda Askell, Sandhini Agarwal, Ariel Herbert-Voss, Gretchen Krueger, Tom Henighan, Rewon Child, Aditya Ramesh, Daniel M. Ziegler, Jeffrey Wu, Clemens Winter, Christopher Hesse, Mark Chen, Eric Sigler, Mateusz Litwin, Scott Gray, Benjamin Chess, Jack Clark, Christopher Berner, Sam McCandlish, Alec Radford, Ilya Sutskever, and Dario Amodei. 2020. Language models are few-shot learners. In *Proceedings of the 34th International Conference on Neural Information Processing Systems (Vancouver, BC, Canada) (NIPS '20)*. Curran Associates Inc., Red Hook, NY, USA, Article 159, 25 pages.
- [14] Nicolas Carion, Francisco Massa, Gabriel Synnaeve, Nicolas Usunier, Alexander Kirillov, and Sergey Zagoruyko. 2020. End-to-End Object Detection with Transformers. In *Computer Vision – ECCV 2020: 16th European Conference, Glasgow, UK, August 23–28, 2020, Proceedings, Part 1 (Glasgow, United Kingdom)*. Springer-Verlag, Berlin, Heidelberg, 213–229. doi:10.1007/978-3-030-58452-8\_13
- [15] Henry Cook, Wesley Terpstra, and Yunsup Lee. 2017. Diplomatic Design Patterns: A TileLink Case Study. In *Proceedings of the First Workshop on Computer Architecture Research with RISC-V (CARRV'17)*. Boston, MA, USA, 1–7.
- [16] Tri Dao. 2023. FlashAttention-2: Faster Attention with Better Parallelism and Work Partitioning. arXiv:2307.08691 [cs.LG] <https://arxiv.org/abs/2307.08691>
- [17] Jacob Devlin, Ming-Wei Chang, Kenton Lee, and Kristina Toutanova. 2019. BERT: Pre-training of Deep Bidirectional Transformers for Language Understanding. In *North American Chapter of the Association for Computational Linguistics*. <https://api.semanticscholar.org/CorpusID:52967399>
- [18] Hasan Genc, Seah Kim, Alon Amid, Ameer Haj-Ali, Vighnesh Iyer, Pranav Prakash, Jerry Zhao, Daniel Grubb, Harrison Liew, Howard Mao, Albert Ou, Colin Schmidt, Samuel Steffl, John Wright, Ion Stoica, Jonathan Ragan-Kelley, Krste Asanovic, Borivoje Nikolic, and Yakun Sophia Shao. 2022. *Gemmini: Enabling Systematic Deep-Learning Architecture Evaluation via Full-Stack Integration*. IEEE Press, 769–774. <https://doi.org/10.1109/DAC18074.2021.9586216>
- [19] Google Cloud. 2019. bfloat16: The secret to high performance on Cloud TPUs. <https://cloud.google.com/blog/products/ai-machine-learning/bfloat16-the-secret-to-high-performance-on-cloud-tpus>. Accessed: 2025-06-27.
- [20] Google Cloud. 2024. *TPU Architecture*. <https://cloud.google.com/tpu/docs/system-architecture-tpu-vm> Accessed: 2025-06-15.
- [21] Google Cloud. 2025. *Cloud TPU v5e Documentation*. <https://cloud.google.com/tpu/docs/v5e> Accessed: 2025-06-15.
- [22] Charles R Harris, K Jarrod Millman, Stéfan J van der Walt, Ralf Gommers, Pauli Virtanen, David Cournapeau, Eric Wieser, Julian Taylor, Sebastian Berg, Nathaniel J Smith, et al. 2020. Array programming with NumPy. *Nature* 585, 7825 (2020), 357–362. doi:10.1038/s41586-020-2649-2
- [23] Muhammad Awais Hussain, Shung-Wei Lin, and Tsung-Han Tsai. 2022. An Area-Efficient and High Throughput Hardware Implementation of Exponent Function. In *2022 IEEE International Symposium on Circuits and Systems (ISCAS)*. 3369–3372. doi:10.1109/ISCAS48785.2022.9937238
- [24] JAX Developers. [n. d.]. JAX Pallas TPU Documentation. <https://docs.jax.dev/en/latest/pallas/tpu/index.html>. Accessed: 2025-06-30.
- [25] Norm Jouppi, George Kurian, Sheng Li, Peter Ma, Rahul Nagarajan, Lifeng Nai, Nishant Patil, Suvinay Subramanian, Andy Swing, Brian Towles, Clifford Young, Xiang Zhou, Zongwei Zhou, and David A Patterson. 2023. TPU v4: An Optically Reconfigurable Supercomputer for Machine Learning with Hardware Support for Embeddings. In *Proceedings of the 50th Annual International Symposium on Computer Architecture (Orlando, FL, USA) (ISCA '23)*. Association for Computing Machinery, New York, NY, USA, Article 82, 14 pages. doi:10.1145/3579371.3589350
- [26] Norman P. Jouppi, Cliff Young, Nishant Patil, David Patterson, Gaurav Agrawal, Raminder Bajwa, Sarah Bates, Suresh Bhatia, Nan Boden, Al Borchers, Rick Boyle, Pierre-luc Cantin, Clifford Chao, Chris Clark, Jeremy Coriell, Mike Daley, Matt Dau, Jeffrey Dean, Ben Gelb, Tara Vazir Ghaemmaghami, Rajendra Gottipati, William Gulland, Robert Hagmann, C. Richard Ho, Doug Hogberg, John Hu, Robert Hundt, Dan Hurt, Julian Ibarz, Aaron Jaffey, Alek Jaworski, Alexander Kaplan, Harshit Khaitan, Daniel Killebrew, Andy Koch, Naveen Kumar, Steve Lacy, James Laudon, James Law, Diemthu Le, Chris Leary, Zhuyuan Liu, Kyle Lucke, Alan Lundin, Gordon MacKean, Adriana Maggiore, Maire Mahony, Kieran Miller, Rahul Nagarajan, Ravi Narayanaswami, Ray Ni, Kathy Nix, Thomas Norrie, Mark Omernick, Narayana Penukonda, Andy Phelps, Jonathan Ross, Matt Ross, Amir Salek, Emad Samadiani, Chris Severn, Gregory Sizikov, Matthew Snelham, Jed Souter, Dan Steinberg, Andy Swing, Mercedes Tan, Gregory Thorson, Bo Tian, Horia Toma, Erick Tuttle, Vijay Vasudevan, Richard Walter, Walter Wang, Eric Wilcox, and Doe Hyun Yoon. 2017. In-Datacenter Performance Analysis of a Tensor Processing Unit. *SIGARCH Comput. Archit. News* 45, 2 (June 2017), 1–12. doi:10.1145/3140659.3080246
- [27] Jared Kaplan, Sam McCandlish, Tom Henighan, Tom B. Brown, Benjamin Chess, Rewon Child, Scott Gray, Alec Radford, Jeffrey Wu, and Dario Amodei. 2020. Scaling Laws for Neural Language Models. arXiv:2001.08361 [cs.LG] <https://arxiv.org/abs/2001.08361>
- [28] Hansung Kim, Ruohan Richard Yan, Joshua You, Tieliang Vamber Yang, and Yakun Sophia Shao. 2025. Virgo: Cluster-level Matrix Unit Integration in GPUs for Scalability and Energy Efficiency. In *Proceedings of the 30th ACM International Conference on Architectural Support for Programming Languages and Operating Systems, Volume 2 (Rotterdam, Netherlands) (ASPLOS '25)*. Association for Computing Machinery, New York, NY, USA, 1382–1399. doi:10.1145/3676641.3716281
- [29] Alexander Kolesnikov, Alexey Dosovitskiy, Dirk Weissenborn, Georg Heigold, Jakob Uszkoreit, Lucas Beyer, Matthias Minderer, Mostafa Dehghani, Neil Houlsby, Sylvain Gelly, Thomas Unterthiner, and Xiaohua Zhai. 2021. An Image is Worth 16x16 Words: Transformers for Image Recognition at Scale.
- [30] Kung. 1982. Why systolic architectures? *Computer* 15, 1 (1982), 37–46. doi:10.1109/MC.1982.1653825
- [31] Long Ouyang, Jeff Wu, Xu Jiang, Diogo Almeida, Carroll L. Wainwright, Pamela Mishkin, Chong Zhang, Sandhini Agarwal, Katarina Slama, Alex Ray, John Schulman, Jacob Hilton, Fraser Kelton, Luke Miller, Maddie Simens, Amanda Askell, Peter Welinder, Paul Christiano, Jan Leike, and Ryan Lowe. 2022. Training language models to follow instructions with human feedback. arXiv:2203.02155 [cs.CL] <https://arxiv.org/abs/2203.02155>
- [32] Adam Paszke, Sam Gross, Francisco Massa, Adam Lerer, James Bradbury, Gregory Chanan, Trevor Killeen, Zeming Lin, Natalia Gimelshein, Luca Antiga, Alban Desmaison, Andreas Köpf, Edward Yang, Zach DeVito, Martin Raison, Alykhan Tejani, Sasank Chilamkurthy, Benoit Steiner, Lu Fang, Junjie Bai, and Soumith Chintala. 2019. *PyTorch: an imperative style, high-performance deep learning*

- library. Curran Associates Inc., Red Hook, NY, USA.
- [33] Pratyush Patel, Esha Choukse, Chaojie Zhang, Aashaka Shah, Iñigo Goiri, Saeed Maleki, and Ricardo Bianchini. 2024. Splitwise: Efficient Generative LLM Inference Using Phase Splitting. In *2024 ACM/IEEE 51st Annual International Symposium on Computer Architecture (ISCA)*. 118–132. doi:10.1109/ISCA59077.2024.00019
- [34] Paul Rosenfeld, Elliott Cooper-Balis, and Bruce Jacob. 2011. DRAMSim2: A Cycle Accurate Memory System Simulator. *IEEE Computer Architecture Letters* 10, 1 (2011), 16–19. doi:10.1109/L-CA.2011.4
- [35] Jay Shah, Ganesh Bikshandi, Ying Zhang, Vijay Thakkar, Pradeep Ramani, and Tri Dao. 2024. FlashAttention-3: Fast and Accurate Attention with Asynchrony and Low-precision. arXiv:2407.08608 [cs.LG] <https://arxiv.org/abs/2407.08608>
- [36] Antonio G.M. Strollo, Davide De Caro, and Nicola Petra. 2011. Elementary Functions Hardware Implementation Using Constrained Piecewise-Polynomial Approximations. *IEEE Trans. Comput.* 60, 3 (2011), 418–432. doi:10.1109/TC.2010.127
- [37] Emma Strubell, Ananya Ganesh, and Andrew McCallum. 2019. Energy and Policy Considerations for Deep Learning in NLP. *ArXiv abs/1906.02243* (2019). <https://api.semanticscholar.org/CorpusID:174802812>
- [38] Ashish Vaswani, Noam Shazeer, Niki Parmar, Jakob Uszkoreit, Llion Jones, Aidan N. Gomez, Lukasz Kaiser, and Illia Polosukhin. 2017. Attention is all you need. In *Proceedings of the 31st International Conference on Neural Information Processing Systems (Long Beach, California, USA) (NIPS'17)*. Curran Associates Inc., Red Hook, NY, USA, 6000–6010.
- [39] C. Wilson. 2024. Verilator: The fastest free Verilog HDL simulator. <https://verilator.org/>. Version 5.024.
- [40] Jianxing Xu, Yuanbo Wen, Zikang Liu, Ruibai Xu, Tingfeng Ruan, Jun Bi, Rui Zhang, Di Huang, Xinkai Song, Yifan Hao, Xing Hu, Zidong Du, Chongqing Zhao, Jiang Jie, and Qi Guo. 2025. Mosaic: Exploiting Instruction-Level Parallelism on Deep Learning Accelerators with iTex Tessellation. In *Proceedings of the 30th ACM International Conference on Architectural Support for Programming Languages and Operating Systems, Volume 2 (Rotterdam, Netherlands) (ASPLOS '25)*. Association for Computing Machinery, New York, NY, USA, 672–688. doi:10.1145/3676641.3716262